Local and Normal Vibrational States: a Harmonically Coupled Anharmonic-oscillator Model

By M. S. Child and R. T. Lawton
Theoretical Chemistry Department, University of Oxford,
1 South Parks Road, Oxford OX1 3TG

Received 8th December, 1980

Analysis of previous calculations indicates that the observation of an irregular overtone/combination spectrum implies increasingly close local-mode near-degeneracies in the higher overtone states. This behaviour is accurately reproduced by a model of two harmonically coupled anharmonic oscillators, when the anharmonicity parameter exceeds the coupling strength, the effect being independent of the momentum or potential origin of the coupling. The same model reproduces familiar normal-mode behaviour in the opposite limit. Applications of the model indicate local-mode behaviour for H_2O and C_2H_2 and normal mode features for C_2D_2 and SO_2, the dominant inter-bond coupling in all cases except H_2O being due to cross-terms in the kinetic-energy operator. In H_2O such momentum coupling is combined with an approximately equal potential coupling contribution.

1. INTRODUCTION

Recent experimental evidence[1-5] for a bond-localised rather than a normal-coordinate picture of X—H stretching vibrations comes from the stability of the higher overtone bands to partial deuteration and from the decreasing overtone bandwidths with increasing excitation. Theoretical interest in a local-mode description of X—H vibrations has a longer history, the main argument until recently[6,7] being that potential coupling between the bonds is relatively unimportant compared with a correctly anharmonic description of the individual bond potentials.[8-12] The tacit assumption here is that the observed frequency splitting between vibrations associated with identical XH bonds is attributable to momentum (*G*-matrix) coupling, but the same argument could be advanced with more justice for vibrations involving heavy peripheral atoms and hence much stronger momentum coupling (the case of SO_2 is discussed below). This suggests that a bond-separable potential model would not be peculiar to XH systems. Moreover, our own quantum-mechanical[7] and classical studies[6,10] have demonstrated a bond localisation of certain vibrational states in a sense akin to that required by the experimental observations[1-5] even in the presence of strong potential coupling between identical bonds.

The purpose of this paper is to argue that localisation in this second sense is attributable to quenching of the interbond coupling by the anharmonicity of the individual bond potentials. To do this we offer a simple model of harmonic momentum and potential coupling between degenerate anharmonic oscillators which is shown to reproduce incipient local-mode features of observed spectra and the more obvious effects shown by our previous extensive numerical calculations.[7] The model also goes over naturally to the familiar normal-coordinate picture in the limit of weak bond anharmonicity, and covers all intermediate cases. The present formulation covers both direct coupling between two identical bonds and indirect coupling through a third degree of freedom, but the model allows extension to any symmetrical system and could be developed to include farther anharmonic coupling terms without disturbing the structure of the theory.

This theory is first set in context in section 2 below, by demonstrating the irregular nature of the overtone/combination spectra of H_2O both as observed experimentally[13-18] and as calculated[19] on the Sorbie–Murrell[20] potential surface. Other localisation characteristics found in previous calculations[6,7] are also briefly reviewed. The model is then developed in section 3 and the predicted characteristics of the overtone spectrum are described in section 4. Applications to H_2O, C_2H_2, C_2D_2 and SO_2 are given in section 5. Finally the main conclusions are summarized in section 6.

2. LOCAL-MODE CHARACTERISTICS

Previous quantal calculations[7] on the stretching vibrations of the Sorbie–Murrell[20] model for water have been extended to include the effect of the bending vibration[19] with very little change in the overall picture.

Fig. 1 shows the disposition of energy levels in the first five overtone manifolds

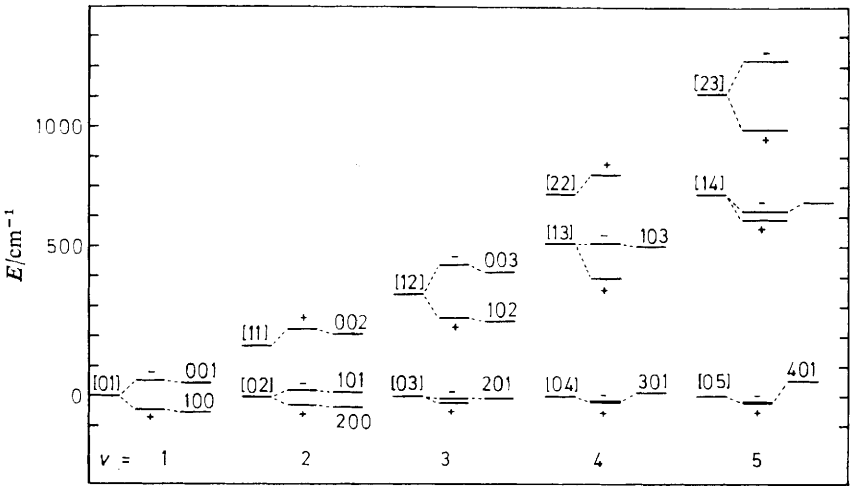

FIG. 1.—Energy levels for the first five $(v_1, 0, v_3)$ overtone manifolds of H_2O. For each manifold index $v = v_1 + v_3$, the figures show (*a*) the Morse energy levels as given by eqn (32), labelled by local mode quantum numbers $[n_a, n_b]$, (*b*) calculated level positions designated $(\pm)$ according to the symmetry under interchange of the bonds, and (*c*) experimental level positions labelled (v_1, v_2, v_3) The energy zero for each manifold is the lowest Morse eigenvalue.

obtained by these extended calculations, and presented in relation to the experimental levels,[13-18] labelled by conventional quantum numbers (v_1, v_2, v_3), and to the levels $[n_a, n_b]$ implied by a separable Morse approximation for each bond, with

$$E_n = (n + \tfrac{1}{2})\hbar\omega - (n + \tfrac{1}{2})^2\hbar x\omega, \tag{1}$$

$(\hbar\omega/\boldsymbol{hc}) = 3876\ \text{cm}^{-1}$, $(\hbar x\omega/\boldsymbol{hc}) = 84.4\ \text{cm}^{-1}$.* The origin for each manifold is taken as the lowest Morse level, measured from the zero-point energy,

$$E[0v] = v\hbar\omega - v(v + 1)\hbar x\omega \tag{2}$$

where $v = v_1 + v_3 = n_a + n_b$. The symbols $\pm$ designate the symmetry with respect to interchange of the two bonds.

The most striking feature is the marked irregularity of the level separations in any given manifold. For example the intervals between successive experimental levels in

* In the notation adopted here, ω and $x\omega$ have dimensions of frequency. $\hbar\omega$ and $\hbar x\omega$ are energies, with equivalent wavenumber units $(\hbar\omega/\boldsymbol{hc})$ and $(\hbar x\omega/\boldsymbol{hc})$.

the $v = 2$ manifold are 49 and 195 cm^{-1}, and the calculated disparities become progressively further exaggerated until the intervals in the $v = 5$ manifold become 0.1, 599, 44, 274 and 224 cm^{-1}. This pattern may be understood in terms of an increased trend towards local mode doubling of adjacent levels as the disparity between the local mode numbers $[n_a, n_b]$ increases. Seen in conjunction with the Morse eigenvalues, this behaviour is plausibly attributed to a perturbation that splits the degeneracies in increasingly high order on moving down any given manifold. This indicates a progressive decoupling between the stretching of the two OH bonds in the very close doublet states.

A second feature, not demonstrated by our previous calculations,[7] which suppressed the bending vibration, is that the magnitudes of the local mode splittings in H_2O are largely unaffected by the level of excitation of this bending mode, as shown in fig. 2.

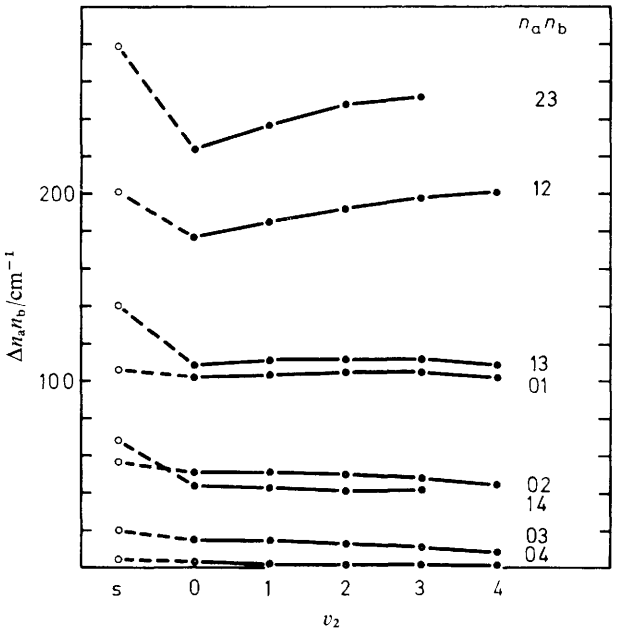

FIG. 2.—Calculated H_2O local-mode splittings $\Delta = E[n_a, n_b^+] - E[n_a, n_b^-]$ as a function of bending quantum number v_2. Points marked by S on the v_2 axis are taken from a stretching-only calculation.[7]

Other local-mode features of previous calculations, but not discussed in detail below are the transition from normal-coordinate to bond-coordinate selection rules as the energy increases,[7] and the spatial localisation of the wavefunction in relation to the classical trajectory relevant to the state in question.[7,12]

3. HARMONICALLY COUPLED DEGENERATE ANHARMONIC OSCILLATORS

DIRECT COUPLING

Direct harmonic coupling between anharmonic oscillators with coordinates (q_a, q_b) may be represented by the Hamiltonian

$$H_{dir} = H_{dir}^{(0)} + H_{dir}^{(1)} \tag{3}$$

with

$$H_{\text{dir}}^{(0)} = \frac{1}{2\mu}(p_a^2 + p_b^2) + V(q_a) + V(q_b) \tag{4}$$

$$H_{\text{dir}}^{(1)} = \frac{1}{\mu_{ab}} p_a p_b + k_{ab}\, q_a q_b. \tag{5}$$

It is assumed for simplicity that any coordinate dependence of the effective masses μ and μ_{ab} can be neglected. The extension to indirect coupling through a third coordinate q_c is outlined below.

Two simple limiting cases may be recognised, the first arising for $H_{\text{dir}}^{(1)} = 0$, when the separability of $H_{\text{dir}}^{(0)}$ implies a doubly degenerate anharmonic oscillator spectrum, as labelled by the local mode labels $[n_a, n_b]$ in fig. 1. The second limit occurs when the anharmonicity of the bond potentials $V(q_v)$ is neglected; thus

$$V(q_v) = \tfrac{1}{2} k q_v^2;\ v = a, b. \tag{6}$$

This leads to the normal-mode picture, with coordinates conventionally labelled (q_1, q_3) for the examples which follow,

$$q_1 = 2^{-\frac{1}{2}}(q_a + q_b),\ q_3 = 2^{-\frac{1}{2}}(q_a - q_b) \tag{7}$$

and harmonic frequencies

$$\nu_1 = \frac{1}{2\pi}\left[\frac{k}{\mu}\left(1 + \frac{k_{ab}}{k}\right)\left(1 - \frac{\mu}{\mu_{ab}}\right)\right]^{\frac{1}{2}} \tag{8}$$

$$\nu_3 = \frac{1}{2\pi}\left[\frac{k}{\mu}\left(1 - \frac{k_{ab}}{k}\right)\left(1 + \frac{\mu}{\mu_{ab}}\right)\right]^{\frac{1}{2}}. \tag{9}$$

Notice for future reference that the two frequencies remain degenerate even in the presence of harmonic coupling if by chance

$$k_{ab}\,\mu_{ab} = k\mu. \tag{10}$$

Even the most minor anharmonic perturbation will lead back to the local-mode picture in this case, showing that the two types of harmonic interbond coupling can act in the same or in opposite senses according to the relative signs of μ_{ab} and k_{ab}.

The model adopted for the anharmonic oscillators is such that the eigenvalues of $H^{(0)}$ are given by the Morse expression:

$$E(n_a, n_b) = \sum_{v=a,b} [(n_v + \tfrac{1}{2})\hbar\omega - (n_v + \tfrac{1}{2})^2 \hbar\omega x]. \tag{11}$$

The coupling matrix elements will, however, be approximated by means of the harmonic oscillator identities

$$p_v|n_v\rangle = -\mathrm{i}(\hbar/2)^{\frac{1}{2}}(\mu k)^{\frac{1}{2}}[-(n_v + 1)^{\frac{1}{2}}|n_v + 1\rangle + n_v^{\frac{1}{2}}|n_v - 1\rangle] \tag{12}$$

$$q_v|n_v\rangle = (\hbar/2)^{\frac{1}{2}}(\mu k)^{-\frac{1}{2}}[(n_v + 1)^{\frac{1}{2}}|n_v + 1\rangle + n_v^{\frac{1}{2}}|n_v - 1\rangle] \tag{13}$$

where k is the effective force constant, $k = \mu\omega^2$, for the unperturbed motion. The corrections required for a full Morse expansion, of order $(\omega x/\omega)$ for the lowest states, are assumed to be at most comparable with those due to inclusion of cubic and higher terms in the potential. As such, they would be required for any attempt to fit the spectrum exactly, but they are not expected to alter the qualitative picture. Eqn (12)

and (13) carry the advantage of $\Delta n_v = 1$ selection rules, and simple analytical matrix elements throughout.

In this approximation the only non-zero coupling matrix elements may be divided into those which couple states within the same ($v = n_a + n_b$) manifold, namely

$$\langle n_a + 1, n_b - 1|H_{dir}^{(1)}|n_a, n_b\rangle = -(\alpha - \beta)[(n_a + 1)n_b]^{\frac{1}{2}}$$
$$\langle n_a - 1, n_b + 1|H_{dir}^{(1)}|n_a, n_b\rangle = -(\alpha - \beta)[n_a(n_b + 1)]^{\frac{1}{2}} \quad (14)$$

and the terms

$$\langle n_a + 1, n_b + 1|H_{dir}^{(1)}|n_a, n_b\rangle = (\alpha + \beta)[(n_a + 1)(n_b + 1]^{\frac{1}{2}}$$
$$\langle n_a - 1, n_b - 1|H_{dir}^{(1)}|n_a, n_b\rangle = (\alpha + \beta)\,[n_a n_b]^{\frac{1}{2}} \quad (15)$$

which couple to states lying at energies approximately $\pm 2\hbar\omega$ above E_{n_a, n_b}, respectively. Here

$$\alpha = \hbar(\mu k)^{\frac{1}{2}}/2\mu_{ab} = \hbar\omega(\mu/2\mu_{ab}),$$
$$\beta = \hbar k_{ab}/2(\mu k)^{\frac{1}{2}} = \hbar\omega(k_{ab}/2k). \quad (16)$$

The first type are taken into account in first order, by constructing a manifold coupling matrix with diagonal elements given by eqn (11) and off-diagonal elements by eqn (14). The second type give rise to a common second-order shift for all diagonal elements in the manifold:

$$E^{(2)} = -\frac{(\alpha + \beta)^2}{2\hbar\omega}(n_a + n_b + 1). \quad (17)$$

INDIRECT COUPLING

The extension to indirect coupling through a third coordinate q_c is achieved by augmenting H_{dir} by a harmonic-oscillator Hamiltonian for the q_c motion and further harmonic-coupling terms. Thus

$$H = H_{dir} + \frac{1}{2\mu_c}p_c^2 + \tfrac{1}{2}k_c q_c^2 - \frac{1}{\mu_{ac}}(p_a + p_b)p_c + k_{ac}(q_a + q_b)q_c. \quad (18)$$

The resulting additional matrix elements are analogous to those given by eqn (14) and (15), but with the coupling strength expressed in terms of

$$\alpha_c = \hbar[\mu k \mu_c k_c]^{\frac{1}{2}}/2\mu_{ac} = (\hbar\omega/\mu_{ac})[\mu\mu_c\omega_c/4\omega]^{\frac{1}{2}}$$

and

$$\beta_c = \hbar k_{ac}/2[\mu k \mu_c k_c]^{\frac{1}{2}} = \hbar\omega\, k_{ac}[\omega_c/4kk_c\omega]^{\frac{1}{2}}, \quad (19)$$

where

$$\omega_c = (k_c/\mu_c)^{\frac{1}{2}}. \quad (20)$$

It is assumed in the model that the magnitude of this coupling is small compared with the energy difference ($\hbar\omega - \hbar\omega_2$) as will normally be the case when $\hbar\omega$ applies to the X—H stretching motion and ω_2 is an H—X—H bending frequency or a stretching frequency involving larger masses. The effect of the indirect coupling may therefore be taken into account by second-order perturbation theory. Again two types of

interaction may be identified. First there is a second-order correction to each unperturbed energy level

$$E^{\circ}(n_a, n_b, n_c) = \sum_{v=a,b} [(n_v + \tfrac{1}{2})\hbar\omega - (n_v + \tfrac{1}{2})^2\hbar x\omega] + (n_c + \tfrac{1}{2})\hbar\omega_c, \tag{21}$$

namely

$$E^{(2)}(n_a, n_b, n_c) = \sum_{n' \neq n} |\langle \boldsymbol{n}|H|\boldsymbol{n}'\rangle|^2/(E_n^{\circ} - E_n^{\circ\prime})$$

$$= -\left(\sum_{v=a,b} \frac{(\alpha_c + \beta_c)^2}{\hbar(\omega + \omega_c)}(n_v + n_c + 1) + \frac{(\alpha_c - \beta_c)^2}{\hbar(\omega - \omega_c)}(n_v - n_c)\right). \tag{22}$$

Secondly the second-order coupling between states $|n_a, n_b, n_c\rangle$ and $|n_a + 1, n_b - 1, n_c\rangle$ gives rise to matrix elements within a given anharmonic manifold of the form

$$\langle n_a + 1, n_b - 1, n_c|H^{(2)}|n_a, n_b, n_c\rangle = [(n_a + 1)n_b]^{\frac{1}{2}}\left\{\frac{(\alpha_c - \beta_c)^2}{\hbar(\omega - \omega_c)} - \frac{(\alpha_c + \beta_c)^2)}{\hbar(\omega + \omega_c}\right\}. \tag{23}$$

Since eqn (22) and (23) have precisely the same dependence on the quantum numbers n_a and n_b as the corresponding direct coupling terms given by eqn (17) and (14) respectively, the effects of both direct and indirect coupling can be taken account by diagonalising a single intramanifold tridiagonal matrix for each $v = n_a + n_b$ level of the system. The elements of the effective hamiltonian are given according to eqn (14), (17), (22) and (23) by

$$\langle n_a, n_b, n_c|H_{eff}|n_a, n_b, n_c\rangle = \sum_{v=a,b} [(n_a + \tfrac{1}{2})\hbar\omega' - (n_a + \tfrac{1}{2})^2\hbar x\omega] + (n_c + \tfrac{1}{2})\hbar\omega_c'$$

$$\langle n_a + 1, n_b - 1, n_c|H_{eff}|n_a, n_b, n_c\rangle = \lambda[(n_a + 1)n_b]^{\frac{1}{2}} \tag{24}$$

where ω' and ω_2' include second-order corrections to the unperturbed frequencies;

$$\omega' = \omega - (\alpha + \beta)^2/2\hbar\omega - (\alpha_c + \beta_c)^2/\hbar(\omega + \omega_c) - (\alpha_c - \beta_c)^2/\hbar(\omega - \omega_c)$$

$$\omega_c' = \omega_c - 2(\alpha_c + \beta_c)^2/\hbar(\omega + \omega_c) + 2(\alpha_c - \beta_c)^2/\hbar(\omega - \omega_c). \tag{25}$$

Similarly the total coupling strength parameter is given by

$$\lambda = -\alpha + \beta + (\alpha_c - \beta_c)^2/\hbar(\omega - \omega_c) - (\alpha_c + \beta_c)^2/\hbar(\omega + \omega_c). \tag{26}$$

Three points are worthy of notice. First the symmetry in n_a and n_b allows an immediate factorisation of H_{eff} into symmetric and antisymmetric parts. Thus the energy distribution in the vth manifold requires at most diagonalisation of two $(v + 1)/2$ dimensional matrices. Secondly both the coupling strength λ and diagonal term differences are independent of the excitation state n_c of the indirect coupling mode. This is consistent with the behaviour shown in fig. 2. Finally eqn (26) shows that the various contributions to λ may act in opposite senses. In particular the case $\alpha = \beta$, $\alpha_c = \beta_c = 0$ corresponds to the situation envisaged in eqn (10), where the two types of harmonic coupling cause a frequency shift without removing the zero-order degeneracy.

4. EIGENVALUE STRUCTURE OF THE OVERTONE MANIFOLD

The nature of the eigenvalue spectrum for any given manifold is readily apparent from the structure of the reduced coupling matrices. These are presented below in symmetrised and antisymmetrised form for $v = 1$-5 using the compact notation $E[n_a, n_b]$ to indicate the appropriate sum of Morse eigenvalues, and $H_{eff}^{\pm}(v)$ for the

coupling matrix itself. The energy dependence on n_c is suppressed, as irrelevant to the level splitting within the manifold.

$$H^{(+)}(1) = E[0, 1] = \lambda; \; H^{(-)}(1) = E[0, 1] - \lambda \tag{27}$$

$$H^{(+)}(2) = \begin{bmatrix} E[0, 2], & 2\lambda \\ 2\lambda, & E[1, 1] \end{bmatrix}; \; H^{(-1)}(2) = E[0, 2]$$

$$H^{(+)}(3) = \begin{bmatrix} E[0, 3], & \sqrt{3}\lambda \\ \sqrt{3}\lambda, & E[1, 2] + 2\lambda \end{bmatrix}; \quad H^{(-)}(3) = \begin{bmatrix} E[0, 3], & \sqrt{3}\lambda \\ \sqrt{3}\lambda, & E[1, 2] - 2\lambda \end{bmatrix} \tag{28}$$

$$H^{(+)}(4) = \begin{bmatrix} E[0, 4], & 2\lambda, & 0 \\ 2\lambda, & E[1, 3], & 2\sqrt{3}\lambda \\ 0, & 2\sqrt{3}\lambda, & E[2, 2] \end{bmatrix}; \quad H^{(-)}(4) = \begin{bmatrix} E[0, 4], & 2\lambda \\ 2\lambda, & E[1, 31] \end{bmatrix} \tag{29}$$

$$H^{(+)}(5) = \begin{bmatrix} E[0, 5], & \sqrt{5}\lambda, & 0 \\ \sqrt{5}\lambda, & E[1, 4], & \sqrt{8}\lambda \\ 0, & \sqrt{8}\lambda, & E[2, 3] + 3\lambda \end{bmatrix}; \; H^{(-)}(5) = \begin{bmatrix} E[0, 5], & \sqrt{5}\lambda, & 0 \\ \sqrt{5}\lambda, & E[1, 4], & \sqrt{8}\lambda \\ 0, & \sqrt{8}\lambda, & E[2, 3] - 3\lambda \end{bmatrix}. \tag{30}$$

The two quantities of importance are the Morse anharmonicity parameter $\hbar x\omega$, which determines the diagonal energy differences, and the coupling strength λ. The nature of the eigenvalue spectrum depends on the ratio between them.

For small $(\lambda/\hbar x\omega)$ there is evidently a first-order splitting between the two $E[0, 1^{\pm}]$, $E[1, 2^{\pm}]$ and $E[2, 3^{\pm}]$ levels respectively, whereas the separation between $E[0, 2^{+}]$ and $E[0, 2^{-}]$ arises only from the second-order interaction of $E[0, 2^{+}]$ with $E[1, 1]$. Similarly in the $v = 3$ manifold $E[0, 3^{+}]$ and $E[0, 3^{-}]$ are separated by the difference in second-order interaction with $E[1, 2^{\pm}]$ which are themselves split by a first-order perturbation. The level splitting $E[0, 3^{+}] - E[0, 3^{-}]$ is therefore of order $(\lambda/\hbar x\omega)^3$. Proceeding to the general case the local-mode splitting of the $[0, v]$ level is of order $(\lambda/\hbar x\omega)^v$. Similar considerations clearly account for the pattern of splittings in fig. 1.

Turning to the opposite limit $\hbar x\omega \ll \lambda$ it is readily verified that the eigenvalues of $H^{(\pm)}(v)$ fall into the sequence

$$E = -v\lambda, \; -(v-2)\lambda, \; \ldots \; v\lambda \tag{31}$$

with a regular spacing of 2λ indicative of the overtone and combination bands arising from two harmonic vibrations with frequencies $(\omega - \lambda)$ and $(\omega + \lambda)$, respectively.

These two limits confirm the behaviour anticipated when the model was introduced. The transition between them is conveniently followed by plotting the general eigenvalues as a function of $(\lambda/x\omega)$ using the reduced notation

$$\varepsilon = [E - \bar{E}(v)]/[\lambda^2 + \hbar^2 x^2 \omega^2]^{\frac{1}{2}} \tag{32}$$

where $\bar{E}(v)$ denotes the mean energy of the vth manifold. The form of such a diagram, given in fig. 3 for $v = 5$, shows the expected transition from doubly degenerate local modes to equally spaced harmonic energy levels, with the local-mode degeneracy persisting to higher $(\lambda/\hbar x\omega)$ values the greater the disparity between the local-mode $[n_a, n_b]$ quantum numbers. The relative order of the symmetric (+) and antisymmetric (—) levels depends on the sign of λ, which is taken here to be positive.

5. APPLICATION TO INDIVIDUAL MOLECULES

In applying the theory to individual molecules our purposes are first to show that the present model can explain the main features of observed and calculated overtone spectra. Secondly we examine the extent to which the implied harmonic coupling

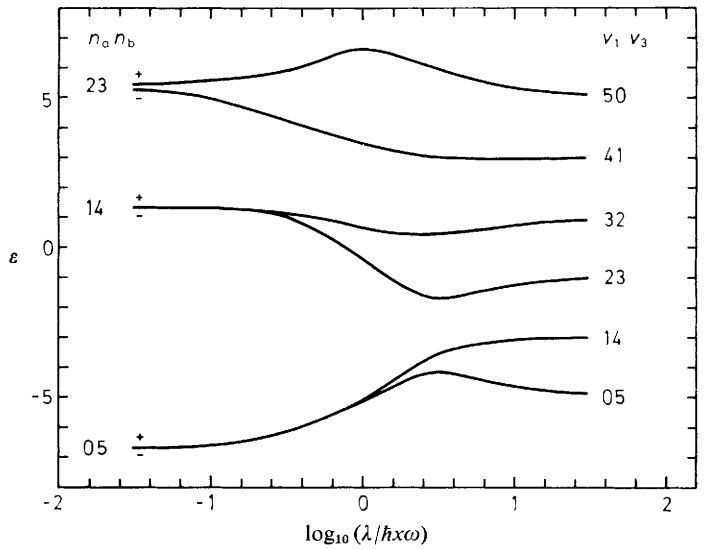

FIG. 3.—Scaled model eigenvalues, $\varepsilon = (E - \bar{E})/(\lambda^2 + \hbar^2 x^2 \omega^2)^{\frac{1}{2}}$ for the $v = 5$ manifold, as a function of $\log_{10}(\lambda/\hbar x\omega)$. $\bar{E}$ is the mean energy of the manifold.

can be attributed to purely momentum coupling, since this bears on the original proposition[8-11] concerning the role of potential coupling between the bonds in the molecule. Finally the model may be used to extrapolate from the observed spectrum, to predict the positions of hitherto unobserved bands.

The four parameters required by the model are the apparent Morse oscillator constants ω' and $x\omega$, the frequency of the indirect coupling mode, ω'_c, (at most one such mode is considered in each case) and the coupling strength λ. These parameters may be derived from the experimental spectrum with levels most conveniently identified by normal-coordinate labels (v_1, v_2, v_3), v_1 and v_3 being taken to refer to the coupled modes and v_2 to the indirect mode. ω'_c is therefore identified with ω_2. The structure of the matrices given by eqn (27)-(30) provides various estimates for the remaining parameters. Thus with all energies measured from the zero-point (0, 0, 0) level, it follows in the light of the correlations between normal- and local-mode labels shown in fig. 1 that

$$\begin{aligned}\lambda &= [E(1, 0, 0) - E(0, 0, 1)]/2 \\ &= [E(3, 0, 0) - E(2, 0, 1) + E(1, 0, 2) - E(0, 0, 3)]/4 \end{aligned} \tag{33}$$

and

$$\begin{aligned}\hbar\omega' - 2\hbar x\omega &= [E(1, 0, 0) + E(0, 0, 1)]/2 \\ \hbar\omega' - 2.5\hbar x\omega &= [E(2, 0, 0) + E(0, 0, 2)]/4 \\ \hbar\omega' - 3\hbar x\omega &= E(1, 0, 1)/2 \\ \hbar\omega' - 4.25\hbar x\omega &= [E(3, 0, 1) + E(1, 0, 3)]/8. \end{aligned} \tag{34}$$

Applications of the theory based on these estimates are given for H_2O, C_2H_2, C_2D_2 and SO_2 below, using the derived parameter values given in table 1.

H_2O

Table 2 gives a comparison between the experimental level positions,[13-17] those given by a new variational calculation[19] on the Sorbie–Murrell[20] surface, including

TABLE 1.—MODEL PARAMETER VALUES

	H_2O	C_2H_2	C_2D_2	SO_2
$(\hbar\omega'/\boldsymbol{hc})/\mathrm{cm}^{-1}$	3876.2	3450.3	2619.4	1271.6
$(\hbar x\omega/\boldsymbol{hc})/\mathrm{cm}^{-1}$	84.4	58.4	23.6	7.5
$(\hbar\omega'_c/\boldsymbol{hc})/\mathrm{cm}^{-1}$	1594.6	1974.3	1764.8	519
$(\lambda/\boldsymbol{hc})/\mathrm{cm}^{-1}$	−49.5	39.0	132.9	−105.2

both stretching and bending vibrations, and finally the levels calculated by the present model. The latter reproduce the experimental and numerical eigenvalues with standard deviations of 7.5 cm^{-1} and 6.3 cm^{-1}, the corresponding standard deviation between numerical and experimental results being 7.1 cm^{-1}. This shows that the model performs remarkably well in reproducing the main features of the spectrum.

It is also illuminating to examine the various contributions to the coupling strength λ, the momentum terms in which may be deduced from knowledge of the valence-coordinate G matrix for a symmetrical XY_2 molecule with bond length r and interbond angle φ[21]

$$G = \begin{bmatrix} \mu_{XY}^{-1}, & m_X^{-1}\cos\varphi, & -(m_X r)^{-1}\sin\varphi \\ m_X^{-1}\cos\varphi, & \mu_{XY}^{-1}, & -(m_X r)^{-1}\sin\varphi \\ -(m_X r)^{-1}\sin\varphi, & -(m_X r)^{-1}\sin\varphi, & 2[m_X + m_Y(1-\cos\varphi)]/m_X m_Y r_2 \end{bmatrix}$$

where μ_{XY} denotes the X—Y reduced mass.

The bond angle φ in H_2O is 104.5°[15] from which it follows using eqn (16) and (19)

TABLE 2.—EXPERIMENTAL NUMERICAL AND MODEL EIGENVALUES FOR H_2O

normal			local			E_{expt}[a]$/\boldsymbol{hc}$	E_{num}[b]$/\boldsymbol{hc}$	$E_{model}/\boldsymbol{hc}$
v_1	v_2	v_3	n_a	n_b	$\pm v_2$	/cm^{-1}	/cm^{-1}	/cm^{-1}
1	0	0	0	1	+0	3 657	3 663	3 658
0	0	1	0	1	−0	3 756	3 765	3 757
2	0	0	0	2	+0	7 201	7 206	7 201
1	0	1	0	2	−0	7 250	7 257	7 246
0	0	2	1	1	0	7 445	7 462	7 460
3	0	0	0	3	+0	—	10 594	10 589
2	0	1	0	3	−0	10 613	10 608	10 600
1	0	2	1	2	+0	10 868	10 877	10 882
0	0	3	1	2	−0	11 032	11 055	11 069
4	0	0	0	4	+0	—	13 800	13 798
3	0	1	0	4	−0	13 831	13 802	13 799
2	0	2	1	3	+0	—	14 213	14 277
1	0	3	1	3	−0	14 319	14 323	14 343
0	0	4	2	2	0	—	14 560	14 559
5	0	0	0	5	+0	—	16 830	16 832
4	0	1	0	5	−0	16 899	16 830	16 832
3	0	2	1	4	+0	—	17 429	17 466
2	0	3	1	4	−0	17 496	17 473	17 505
1	0	4	2	3	+0	—	17 745	17 792
0	0	5	2	3	−0	—	17 971	18 049

[a] Ref. (13)-(18); [b] ref. (19).

that $\alpha/hc = 28.6\ \text{cm}^{-1}$ and $\alpha_c/hc = 49.7\ \text{cm}^{-1}$, giving a direct momentum contribution of $-28.6\ \text{cm}^{-1}$ to the total coupling strength $\lambda/hc = -49.5\ \text{cm}^{-1}$, but a negligible indirect term of $+0.63\ \text{cm}^{-1}$ because according to eqn (26), α_c contributes to λ only in second-order. Information on the division of the residual potential coupling is available by comparison between the present calculation and previous stretching-only calculations,[7] which would be fit by $\lambda/hc = -53\ \text{cm}^{-1}$. The difference of $+4\ \text{cm}^{-1}$ it therefore attributable to indirect potential coupling, leaving $-19.9\ \text{cm}^{-1}$ due to direcs potential coupling between the bonds.

C_2H_2 AND C_2D_2

The available experimental information[15,22-26] on the $(v_i, 0, v_3)$ levels of acetylene and deuteroacetylene is summarised in table 3.

TABLE 3.—EXPERIMENTAL AND MODEL EIGENVALUES FOR C_2H_2, C_2D_2, SO_2

normal			local			C_2H_2		C_2D_2		SO	
v_1	v_2	v_3	n_a	$n_c \pm v_2$		E_{expt}^{a}/hc /cm^{-1}	E_{model}/hc /cm^{-1}	E_{expt}^{b}/hc /cm^{-1}	E_{model}/hc cm^{-1}	E_{expt}/hc /cm^{-1}	E_{model}/hc /cm^{-1}
1	0	0	0	1	+0	3 373	3 373	2 705	2 705	1 151	1 151
0	0	1	0	1	−0	3 295	3 295	2 439	2 439	1 362	1 362
2	0	0	0	2	+0	6 502	6 511	—	4 854	2 296	2 295
1	0	1	0	2	−0	6 556	6 550	5 097	5 097	2 500	2 498
0	0	2	1	1	0	6 709	6 706	—	5 388	2 715	2 716
3	0	0	0	3	+0	—	9 636	—	7 463	3 431	3 431
2	0	1	0	3	−0	9 640	9 625	—	7 244	3 630	3 627
1	0	2	1	2	+0	—	9 976	—	8 047	—	3 838
0	0	3	1	2	−0	9 835	9 831	7 734	7 735	4 054	4 063
4	0	0	0	4	+0	—	12 615	—	9 608	—	4 560
3	0	1	0	4	−0	12 676	12 617	9 794	9 801	4 751	4 747
2	0	2	1	3	+0	—	12 910	—	10 055	—	4 951
1	0	3	1	3	−0	—	13 001	10 348	10 351	5 166	5 170
0	0	4	2	2	0	—	13 192	—	10 684	—	5 403
5	0	0	0	5	+0	—	15 484	—	12 111	—	5 906
4	0	1	0	5	−0	(15 600)[d]	15 484	11 905	11 946	—	6 085
3	0	2	1	4	+0	—	15 951	—	12 628	—	6 282
2	0	3	1	4	−0	—	15 914	12 344	12 347	—	6 495
1	0	4	2	3	+0	—	16 350	—	13 297	—	6 721
0	0	5	2	3	−0	—	16 153	—	12 946	—	6 961

[a] Ref. (15) and (22)-(24); [b] ref. (15) and (24)-(26); [c] ref. (27) and (28); [d] assigned as (0, 0, 5)–(0, 0, 0) band in Herzberg.[15]

Notice that the coupling strength λ given in table 2 is now positive, thereby reversing the order of symmetric and antisymmetric levels from that in fig. 1 and table 2. Secondly λ is larger and the anharmonicity $\hbar x\omega$ is smaller in C_2D_2 than in C_2H_2, a difference that profoundly affects the relative natures of the overtone spectra. As seen in table 3 and fig. 4 the spectrum of C_2H_2 shows qualitatively the same local-mode doublet structure as that encountered in the case of H_2O. The spectrum of C_2D_2 on the other hand is much more " normal " in nature with an almost uniform variation in the intervals between successive levels.

Part of this difference in character is due to the change in bond anharmonicity, roughly in inverse proportion to the change in C—H reduced mass as required by a strict interpretation of the model. The major change is, however, due to the greatly

increased coupling strength λ in C_2D_2 arising from the relatively near resonance between the stretching frequencies of the C—D and C—C bonds, the dominant contribution to λ being indirect momentum coupling generated by the G matrix

$$G = \begin{bmatrix} \mu_{CH}^{-1}, & 0, & -m_C^{-1} \\ 0 & \mu_{CH}^{-1}, & -m_C^{-1} \\ -m_C^{-1} & -m_C^{-1}, & \mu_{CC}^{-1} \end{bmatrix}. \tag{36}$$

Thus in the notation of eqn (18), $\mu_{ac} = m_c/2$. It follows from eqn (19) and the values of ω' in table 2 that $\alpha_c/\boldsymbol{hc} = 262$ and $306\ cm^{-1}$ in C_2H_2 and C_2D_2, respectively, but this relatively small difference is greatly exaggerated in its second-order effect, as given by eqn (26). The resulting indirect momentum coupling contributions are $40\ cm^{-1}$ for

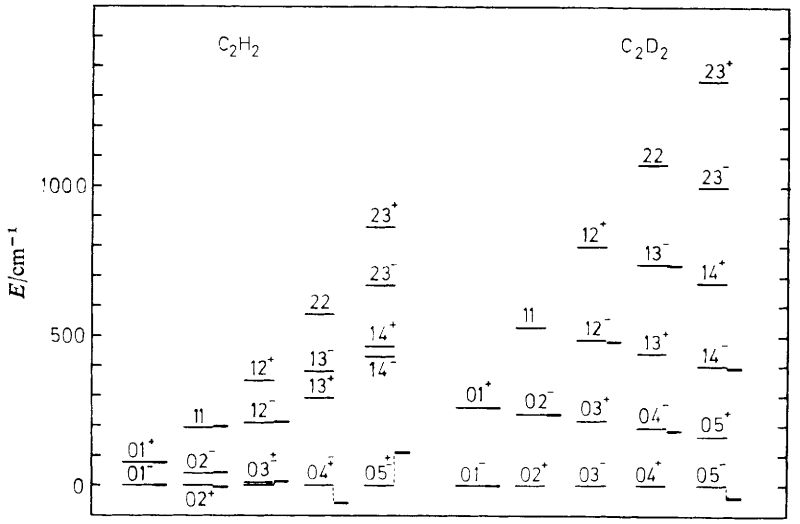

FIG. 4.—Calculated eigenvalues for the first five CH/CD stretching overtone manifolds for C_2H_2 and C_2D_2, designated by local mode labels $[n_a, n_b]$. Short heavy lines mark available experimental levels. Energies are measured in each manifold from the lowest calculated level (see table 3).

C_2H_2 and $197\ cm^{-1}$ for C_2D_2 after correcting the " observed " frequencies ω' and ω'_c in table 1 for the second-order shifts given in eqn (25). The corresponding values for $\lambda/\boldsymbol{hc}$ in table 1 are 39 and $133\ cm^{-1}$. This shows that the coupling in C_2H_2 is entirely attributable to the indirect momentum terms involving α_c eqn (26). The same is almost certainly true for C_2D_2, the overestimate obtained being attributable to the breakdown of second-order perturbation theory. In any case the substantial qualitative difference between the two overtone spectra is well-accounted for by the model.

SO_2

The case of SO_2 is of interest in completing the transition from local-mode behaviour in H_2O and C_2H_2 to an extremely regular normal-mode overtone spectrum. The very large coupling parameter $\lambda/\boldsymbol{hc} = -105\ cm^{-1}$ would seem to dominate the very small anharmonicity $(\hbar x\omega/\boldsymbol{hc}) = 7.53\ cm^{-1}$ given in table 2, but this anharmonicity is in fact required to account for the minor variations in level spacings shown in table 3. Thus the present model again gives a good fit to the experimental level positions.

Finally it is readily verified by substituting the appropriate masses in the matrix

given by eqn (41) that with the bond angle $\varphi = 119.3°$, the direct momentum coupling contribution to $\lambda/\boldsymbol{hc}$ is -102.5 cm^{-1} which may be compared with the full value of -105 cm^{-1}. We therefore have a good representation of a completely " normal " spectrum, reproduced within a bond separable potential model.

6. SUMMARY AND CONCLUSIONS

It has been argued that the observation of a markedly irregular overtone spectrum for a symmetrical molecule should be interpreted as a sign of incipient decoupling between symmetry related bond vibrations in certain states, such decoupling beiog predicted to increase with further excitation. The cause of this decoupling was shown to be strong bond anharmonicity which can in favourable cases quench any interbond coupling terms arising either from potential- or kinetic-energy terms in the Hamiltonian. Thus local-mode behaviour should not be associated with a bond-separable potential approximation.

A model embodying bond anharmonicity and both direct and indirect harmonic coupling between two bonds was introduced, and applied to the stretching spectra of H_2O, C_2H_2, C_2D_2 and SO_2. The important parameter in the model is the ratio of coupling strength to bond anharmonicity, very large and very small values of which give rise to " near-normal " and " near-local " behaviour, respectively. Of the molecules considered H_2O and C_2H_2 lay towards the local limit, while C_2D_2 and SO_2 showed more normal behaviour.

Analysis of the origin of the interbond coupling showed that in H_2O the dominant and roughly equally important mechanisms were direct potential and momentum coupling. Indirect coupling *via* the bending mode was relatively unimportant. In C_2H_2 and C_2D_2 the important term was indirect momentum coupling *via* the C—C stretching mode, this second-order effect being much stronger in C_2D_2 than in C_2H_2 due to the closer resonance between C—D and C—C vibrational frequencies. Finally in SO_2 direct momentum coupling between the bonds was sufficient to quench the weak bond anharmonicity, and to reproduce the experimental spectrum.

Finally it should be recognised that the predicted increasingly near degeneracy with increasing excitation in the lowest local-mode progressions of H_2O and C_2H_2 remains to be tested experimentally. Direct observation of the effect is in principle possible in the infrared overtone spectrum of H_2O because both symmetric and anti-symmetric stretching modes are infrared active. The analysis is, however, complicated by the large rotational constants, principally due to strong Coriolis interaction, but also because the rotational envelope width $(\boldsymbol{BkT})^{\frac{1}{2}} \simeq 100$ cm^{-1} exceeds even the predicted $[03^{\pm}]$ band origin separation by an order of magnitude. In the case of C_2H_2 on the other band direct information on the highly excited Σ_g CH stretching states would be available only from the Raman overtone spectrum.

The authors are grateful for discussions with and some computational assistance from Dr. L. Halonen.

[1] R. L. Swofford, M. E. Long and A. C. Albrecht, *J. Chem. Phys.*, 1976, **65**, 179.
[2] R. L. Swofford, M. E. Long, M. S. Burberry and A. C. Albrecht, *J. Chem. Phys.*, 1977, **66**, 664.
[3] R. L. Swofford, M. S. Burberry, J. A. Morrell and A. C. Albrecht, *J. Chem. Phys.*, 1977, **66**, 5245.
[4] J. N. Perry and A. H. Zewail, *Chem. Phys. Lett.*, 1979, **65**, 31.
[5] R. G. Bray and M. J. Berry, *J. Chem. Phys.*, 1979, **71**, 4909.
[6] R. T. Lawton and M. S. Child, *Mol. Phys.*, 1979, **37**, 1799.
[7] R. T. Lawton and M. S. Child, *Mol. Phys.*, 1980, **40**, 773.

[8] See B. R. Henry, *Acc. Chem. Res.*, 1977, **10**, 207.
[9] R. Wallace, *Chem. Phys.*, 1975, **11**, 189.
[10] M. L. Elert, P. R. Stannard and W. M. Gelbart, *J. Chem. Phys.*, 1977, **67**, 5395.
[11] W. M. Gelbart, P. R. Stannard and M. L. Elert, *Int. J. Quant. Chem.*, 1978, **14**, 703.
[12] R. T. Lawton and M. S. Child, to be published.
[13] R. Mecke, *Z. Phys.*, 1933, **81**, 313.
[14] K. Frendenberg and R. Mecke, *Z. Phys.*, 1933, **81**, 465.
[15] G. Herzberg, *Infrared and Raman Spectra*, 1948, **74**, 703.
[16] O. C. Mohler and W. S. Benedict, *Phys. Rev.*, 1948, **74**, 702.
[17] R. C. Nelson and W. S. Benedict, *Phys. Rev.*, 1948, **74**, 703.
[18] W. S. Benedict, *Phys. Rev.*, 1948, **74**, 1246A.
[19] R. T. Lawton, *D.Phil. Thesis* (Oxford University, 1980).
[20] K. S. Sorbie and J. N. Murrell, *Mol. Phys.*, 1975, **29**, 1387.
[21] E. B. Wilson, J. C. Decius and P. C. Cross, *Molecular Vibrations* (McGraw-Hill, N.Y., 1955).
[22] E. K. Plyler, E. D. Tidwell and T. A. Wiggins, *J. Opt. Soc. Am.*, 1963, **53**, 589.
[23] W. J. Lafferty and R. J. Thibault, *J. Mol. Spectrosc.*, 1964, **14**, 79.
[24] H. Fast and H. L. Welsh, *J. Mol. Spectrosc.*, 1972, **41**, 203.
[25] O. D. Saksena, *J. Chem. Phys.*, 1952, **20**, 95.
[26] R. M. Talley and A. H. Nielson, *J. Chem. Phys.*, 1954, **22**, 2030.
[27] R. D. Shelton and A. H. Nielson, *J. Chem. Phys.*, 1953, **21**, 2178.
[28] R. D. Shelton, A. H. Neilson and W. H. Fletcher, *J. Chem. Phys.*, 1954, **22**, 1731.